March 14, 2018
Volume 140
Number 10
pubs.acs.org/JACS

JACS

JOURNAL OF THE AMERICAN CHEMICAL SOCIETY

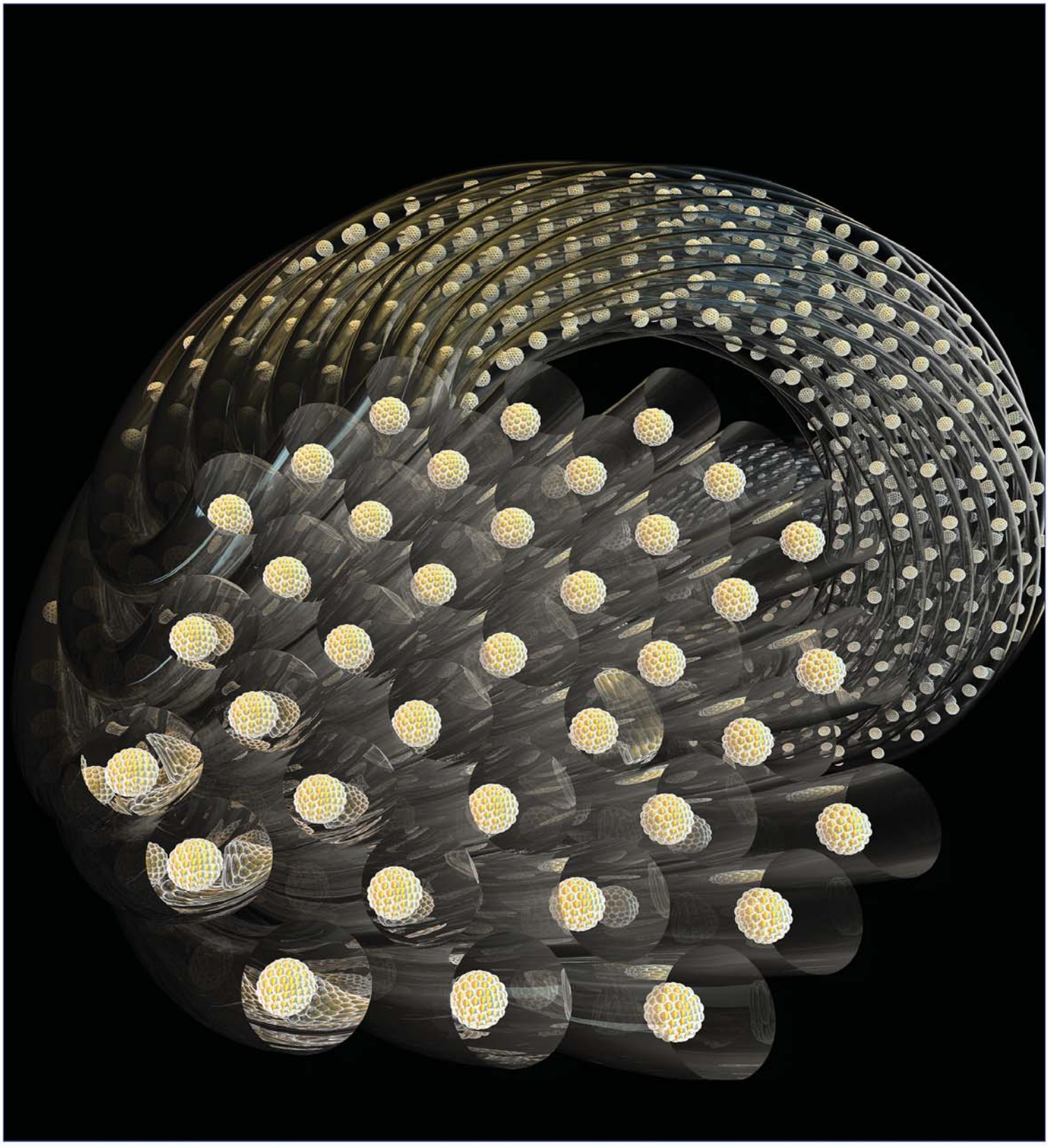

ACS Publications
Most Trusted. Most Cited. Most Read.

www.acs.org

JACS
JOURNAL OF THE AMERICAN CHEMICAL SOCIETY
Article
Cite This: J. Am. Chem. Soc. 2018, 140, 3652−3662
pubs.acs.org/JACS

Mesophase Formation Stabilizes High-Purity Magic-Sized Clusters

Douglas R. Nevers,[†,§] Curtis B. Williamson,[†,§] Benjamin H. Savitzky,[+] Ido Hadar,[#] Uri Banin,[#] Lena F. Kourkoutis,[∥,⊥] Tobias Hanrath,[*,†] and Richard D. Robinson[*,‡]

[†]Robert F. Smith School of Chemical and Biomolecular Engineering, Cornell University, Ithaca, New York 14850, United States
[+]Department of Physics, Cornell University, Ithaca, New York 14850, United States
[#]The Institute of Chemistry and Center for Nanoscience and Nanotechnology, The Hebrew University of Jerusalem, Jerusalem 91904, Israel
[∥]School of Applied and Engineering Physics, Cornell University, Ithaca, New York 14850, United States
[⊥]Kavli Institute for Nanoscale Science, Cornell University, Ithaca, New York 14850, United States
[‡]Department of Materials Science and Engineering, Cornell University, Ithaca, New York 14850, United States

Supporting Information

ABSTRACT: Magic-sized clusters (MSCs) are renowned for their identical size and closed-shell stability that inhibit conventional nanoparticle (NP) growth processes. Though MSCs have been of increasing interest, understanding the reaction pathways toward their nucleation and stabilization is an outstanding issue. In this work, we demonstrate that high concentration synthesis (1000 mM) promotes a well-defined reaction pathway to form high-purity MSCs (>99.9%). The MSCs are resistant to typical growth and dissolution processes. On the basis of insights from *in situ* X-ray scattering analysis, we attribute this stability to the accompanying production of a large (>100 nm grain size), hexagonal organic−inorganic mesophase that arrests growth of the MSCs and prevents NP growth. At intermediate concentrations (500 mM), the MSC mesophase forms, but is unstable, resulting in NP growth at the expense of the assemblies. These results provide an alternate explanation for the high stability of MSCs. Whereas the conventional mantra has been that the stability of MSCs derives from the precise arrangement of the inorganic structures (i.e., closed-shell atomic packing), we demonstrate that anisotropic clusters can also be stabilized by self-forming fibrous mesophase assemblies. At lower concentration (<200 mM or >16 acid-to-metal), MSCs are further destabilized and NPs formation dominates that of MSCs. Overall, the high concentration approach intensifies and showcases inherent concentration-dependent surfactant phase behavior that is not accessible in conventional (i.e., dilute) conditions. This work provides not only a robust method to synthesize, stabilize, and study identical MSC products but also uncovers an underappreciated stabilizing interaction between surfactants and clusters.

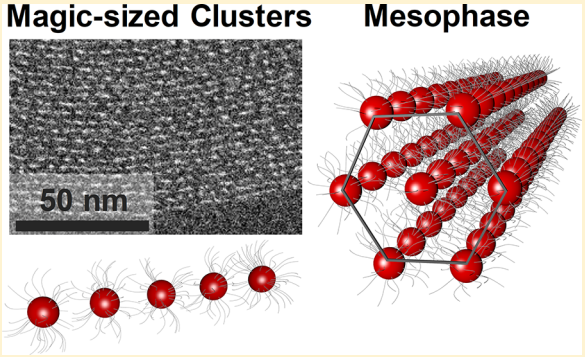

INTRODUCTION

Traditionally, colloidal nanoparticle (NP) synthesis is characterized by solely tracking the evolution of the inorganic materials from precursor conversion to monomers and, ultimately, to NPs.[1−4] Recent studies demonstrate that the organic surfactants play a central role during NP synthesis by controlling the precursor solubility and reactivity.[1,2,5−8] In addition to these critical functions, the NP cation precursors alone, as an isolated system, also exhibit well-established surfactant phase behavior, even at elevated temperatures (>100 °C), and were previously known as heavy metal soaps (i.e., metal carboxylates).[6,9,10] Only recently has the surfactant behavior of NP precursors become appreciated within the NP field.[6,11−13]

For instance, Buhro and co-workers reported that, at lower temperatures, magic-sized clusters (MSCs), which are a single sized nanomaterial, form within a lamellar surfactant mesophase or liquid crystalline structure that is composed of the precursors.[11,12,14] Mesophases are partially ordered structures (e.g., liquid crystals) and are characterized by a turbid solution,[15] well-defined peaks in small-angle X-ray scattering (SAXS),[16,17] and/or optical birefringence.[18] Based on these metrics, several studies have alluded to a connection between surfactant structure and MSC formation, such as the observation of solution turbidity and the self-assembly of MSCs,[19] or detection of large (∼1 nm) micellar aggregates.[20,21] These results suggest that previous studies may have been, unknowingly, observing surfactant phase behavior, and in some cases mesophase formation, coupled with MSC formation.

MSCs are generally suspected to form in syntheses with higher levels of monomer supersaturation, when precursor

Received: November 17, 2017
Published: January 27, 2018

© 2018 American Chemical Society

DOI: 10.1021/jacs.7b12175
J. Am. Chem. Soc. 2018, 140, 3652−3662

conversion kinetics are faster than the nucleation rate, and to function as a reservoir for monomer.[22−27] Previous studies have achieved high levels of supersaturation, and thus promoted MSCs formation, through lower synthesis temperatures (in some cases, <100 °C),[11,12,14,21,22,28,29] and low acid-to-metal ratios (~3).[19,25,30−32] If temperatures are sufficiently low (or concentration sufficiently high), monomeric surfactants can assemble into micelles or mesophases based on micelle theory (i.e., above the critical micelle temperature/concentration). This behavior is analogous to NP nucleation from monomer at sufficiently high supersaturation (i.e., critical nucleation temperature/concentration). Hence, the high supersaturation (of both surfactants and inorganic species) during MSC formation may relate to surfactant phase behavior. Though lower temperatures have been directly investigated to achieve higher supersaturation and thus promote MSC formation,[11,12,14,21,28] the importance of high precursor (and thus metal surfactant) concentrations and its relationship to surfactant mesophases have not yet been established.

In this paper we address the outstanding question: how does the precursor concentration direct the synthetic pathway between NPs and MSCs? We show that high precursor (or metal surfactant) concentrations preferentially promote MSCs formation and suppress NP growth. We attribute the suppression of NP growth to the formation of fibrous mesophase assemblies consisting of MSCs and organics, effectively shielding the MSC nuclei from the reaction solution (Figure 1). By following the evolution of both organic and inorganic constituents, through a combined analysis of *in situ* NMR and X-ray scattering and *ex situ* optical spectroscopy and electron microscopy, we discovered that, upon formation of MSCs in highly concentrated solutions, long-range mesophase structures (100s of nm) are formed. In contrast to previous studies at lower temperatures (<100 °C),[11,12,14,21,28] we demonstrate that MSCs exist within a mesophase structure at elevated temperatures (~130 °C). Our results reinforce an emerging understanding that the stability, or resistance to growth, of MSCs originates from a surfactant (or ligand) mesophase or coordination network, in spite of the atomic arrangement of cluster core. We show that high precursor concentration promotes highly selective nucleation of a single MSC species. We leverage the highly selective reaction to directly probe and track the kinetics of the MSC synthesis. Overall, high concentrations accentuate surfactant phase behavior promoting the formation of high-purity MSCs along with a stabilizing hexagonal mesophase.

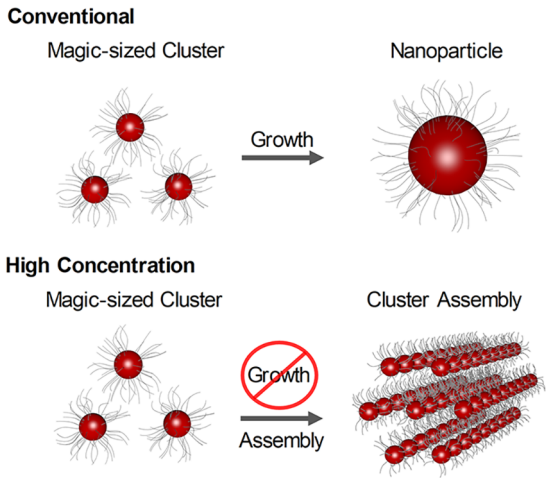

Figure 1. Synthesis pathways. Schematic illustrating the fundamental differences in reaction pathways between conventional (100 mM) synthesis and high concentration (1000 mM) synthesis. For conventional synthesis, nucleation and growth occur simultaneously; in contrast, at high concentrations, the synthesis stops after the MSC formation/nucleation because of the formation of a MSC assembly.

RESULTS

Synthesis Concentration. The concentration of the precursors controls the reaction pathways: at lower concentrations both NPs and MSCs are formed, whereas at higher concentrations MSC formation is promoted and NP growth is suppressed. We used a simplified organic synthesis involving only cadmium oleate, oleic acid, and tri-*n*-octylphosphine sulfide (TOP=S) in a one-pot, heat-up method (see SI for additional details). We investigated three different cadmium oleate concentrations (100, 500, and 1000 mM), with the balance of the solution being oleic acid and TOP=S (2500 mM TOP=S; stoichiometric ratio 2:1 Cd:S). At high concentrations (500 and 1000 mM), absorption spectra of the cleaned product show a single, narrow (111 meV fwhm) excitonic peak at 324 nm (Figure 2a, note log scale on vertical axis). Synthesis at conventional concentrations (100 mM) does not show an excitonic peak. We previously determined the composition of these MSCs as predominately organic (70 wt %), with a 2:1 Cd:S ratio, and a repeat formula unit of $[(CdS)Cd(OA)_2]_x$ (where OA is oleic acid).[33] Based on an empirical sizing curve,[34] the peak at 324 nm corresponds to a particle size of 1.64 ± 0.05 nm. The small deviation in size (which is approximately 1/5th of a Cd−S bond) suggests that each cluster has an identical number of Cd atoms. From published data on similar CdS clusters, we estimate the number of Cd atoms per cluster to be between 17 to 32 atoms.[35−40]

Over the course of the 1000 mM reaction (6 h at 130 °C), the peak at 324 nm increases in intensity but does not shift, indicating continuous formation of MSCs (Figure S1). At the highest concentration, 1000 mM, the peak at 324 nm is dominant with only a small contribution from a broad NP peak (~300 meV fwhm) that shifts during growth from 375 to 404 nm (NPs account for <0.1% of total product based on particle concentration, see SI). For the 500 mM reaction, the NP peak that accompanies the MSC, 324 nm, peak is more intense compared to the 1000 mM reaction and located at 387 nm (fwhm ~ 200 meV). The broad peak is a signature of polydisperse, continuous growth NPs; the 387 nm peak corresponds to 3.0 ± 0.5 nm diameter NPs.[34] Over the course of the 500 mM reaction (6 h at 130 °C), the MSC peak at 324 nm increases and then decreases in intensity but does not shift (Figure S1). This increase and decrease in intensity without a peak shift indicates the MSCs are increasing and decreasing in number but their size is not changing. Concomitantly, the reduction of the MSCs peak corresponds to a shift (358 to 418 nm) in the broad NP peak. By converting the peak intensity to concentration of MSCs and NPs, using a size-dependent extinction coefficient,[34] we can quantify the purity of the MSC product relative to the NPs (see SI for purity calculation; note the purity calculation assumes the empirical extinction coefficient and sizing curve are accurate for ultrasmall particles). These results show that higher precursor concentrations result in a higher purity of MSCs product, specifically 99.1% and 99.9% for the uncleaned products of the 500 and 1000 mM

DOI: 10.1021/jacs.7b12175
J. Am. Chem. Soc. 2018, 140, 3652−3662

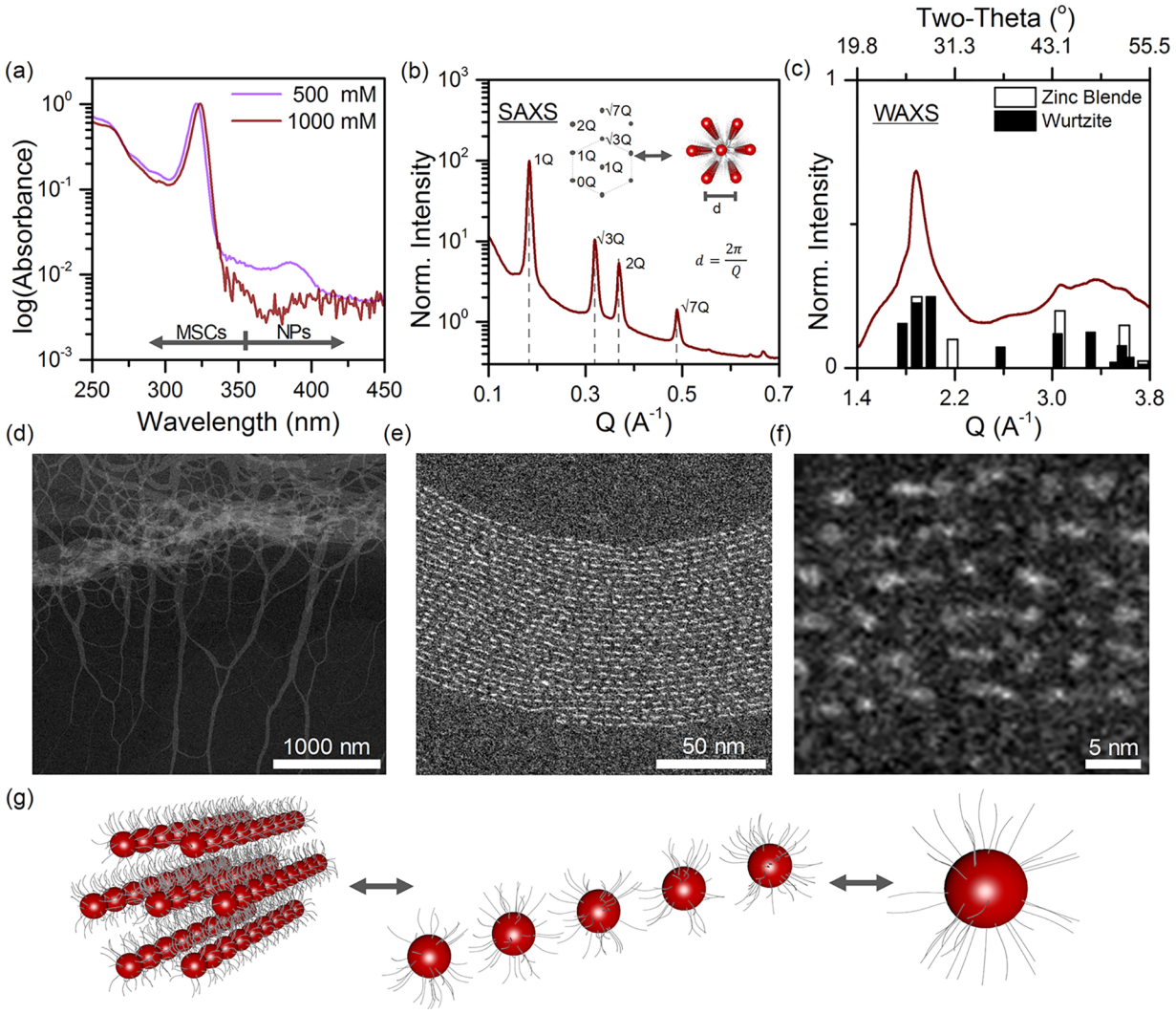

Figure 2. MSC electronic and physical structure. (a) Log of absorbance for cleaned magic-sized clusters prepared at two different metal precursor concentrations (500 and 1000 mM). (b) SAXS of 1000 mM MSC synthesis at 6 h at 130 °C. Inset: reciprocal and real space model of hexagonal MSC assembly. (c) WAXS of 1000 mM MSC synthesis at 6 h at 130 °C compared to zinc blende (PDF#00−010−0454) and wurtzite (PDF#00-041-1049) CdS reference peaks. (d−f) STEM images of MSCs. (d) Long (>1 μm) bundles of fibers composed of MSCs. (e) Zoomed-in view of fibers (3.4 nm *d*-spacing, Figure S3). (f) discrete MSCs (1−2 nm) within a fiber. (g) Schematic of the MSC hexagonal mesophase. The mesophase (left) is an assembly of nanofibers (center), which are composed of magic-sized clusters (right).

reactions, respectively. After cleaning (see SI for details) the 1000 mM reaction, there is no detection of a NP peak (purity > 99.9%; see Figure S1b). At the same conditions, the conventional concentration (100 mM) does not produce MSCs or NPs. (Note: upon cooling from 130 °C or further heating to 200 °C (see SI), NPs precipitate.) Thus, precursor concentration tunes the synthesis selectivity from no products to high-purity MSCs.

Mesophase Structure. The observed preference for high-purity MSCs at high concentrations raises the question: what stabilizes MSCs in solution and what prevents the transition to NP growth? The answer detailed below is based on the stabilization derived from changes in the surfactant (e.g., cadmium oleate) phase behavior at high surfactant concentration. Mesophase formation is suggested by the increased turbidity (caused by light scattering with large particulates) in the solution upon MSC formation (Figure 3). Notably, the stability of MSCs at high concentration enables their large-scale production and isolation (Figure 3). *In situ* small- and wide-angle X-ray scattering (SAXS/WAXS) at 130 °C for the 1000 mM reaction confirm the formation of well-ordered mesoscale assemblies (Figure 2b) and small inorganic crystal domains (Figure 2c). The combination of SAXS and WAXS is particularly powerful because SAXS captures larger mesophases, whereas WAXS examines the individual MSCs. For the 1000 mM reaction, SAXS shows several narrow peaks while several broad peaks are detected in WAXS. The narrow SAXS peak signatures are characteristic of hexagonal spacing in reciprocal space (Q spacing of the peaks is $1:\sqrt{3}:2:\sqrt{7}$; the corresponding Miller indices are 100, 110, 200, and 210, respectively; see Figure 2b). The first hexagonal mesophase peak ($1Q \sim 0.1845$ Å^{-1}) corresponds to a 3.4 nm *d*-spacing, and has an extremely large mesophase crystallite size, >170 nm (see SI for details; the peak width is dominated (~86%) by instrumental broadening). The change in slope at low Q (0.1−0.2 Å^{-1}) corresponds to the NP structure factor. The peaks in the WAXS from the MSCs align with the diffraction planes for cadmium sulfide, and most closely with the wurtzite (WZ) phase (Figure 2c). For instance, the weak peak at 2.6 Å^{-1} represents a characteristic (102) wurtzite plane, corresponding

DOI: 10.1021/jacs.7b12175
J. Am. Chem. Soc. 2018, 140, 3652−3662

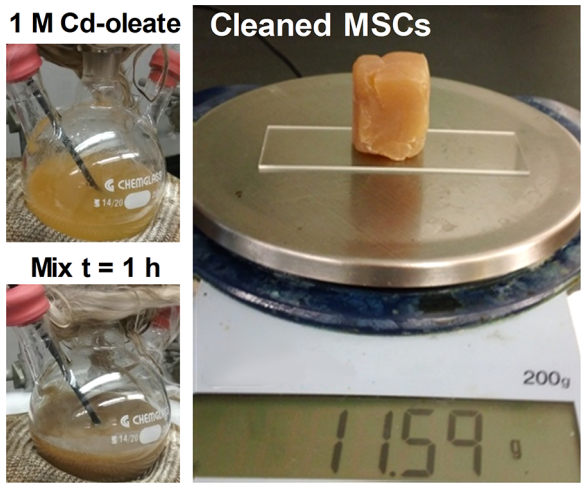

Figure 3. MSC turbidity and scale-up. Upon MSC formation at 140 °C, the cadmium oleate + TOP=S mixture transforms from a translucent orange solution (similar to Cd-oleate only solution) to a turbid tan solution (from top to bottom). The right image is the 11.6 g of cleaned MSCs produced from a 100 mL 1000 mM reaction (~30% inorganic mass[33]). Conversion is ~25% after 1 h.

to $2\theta = 36.6°$ for a Cu-α radiation, which is absent in the zinc blende (ZB) phase. The observation of the more thermodynamically stable WZ phase under kinetically controlled conditions is consistent with computational work that show phase stability to be dependent on size and surface termination (for Cd-terminated, as is the case here, WZ is preferred),[41,42] as well as demonstrate polytypism in WZ/ZB systems depending on prepration.[43] The breadth of the WAXS peaks suggests the MSCs have a ~2 nm crystallite (Figure S2), which is much smaller than the mesophase grain size (>170 nm), indicating that a mesophase grain contains thousands of MSCs.

To better understand the fundamental link between the MSC stability, or their resistance to form NPs, and their mesoscale structure we imaged the cleaned 1000 mM MSC synthesis product using aberration corrected scanning transmission electron microscopy (STEM) (Figure 2d–f, see SI). Unexpectedly, the STEM images reveal long (~10s μm), fibrous assemblies with ~3.5 nm interfiber spacing (Figure 2d–f and Figure S3). The interfiber spacing based on STEM is consistent with the 3.4 nm *d*-spacing of the first hexagonal mesophase peak (Figure S3). Closer inspection reveals that the fibers are not continuous inorganic wires, but consist of discrete inorganic entities, each ~2 nm in size. During high resolution STEM imaging, the clusters restructure and degrade quickly under electron irradiation, which has prevented more detailed, atomic-level imaging (see Figure S4). Overall, the size of these entities observed via STEM is similar to the size determined from WAXS (~2.2 ± 0.9 nm, Figure S2) and absorption spectroscopy (1.64 ± 0.05 nm, based on empirical sizing curve[34]). We summarize the hierarchical arrangement of MSCs within fibers, and fibers within hexagonal mesophase in Figure 2g. The lack of a hexagonal mesophase in the STEM data suggests that the mesophase structure unbundles upon dilution, and indicates that the improved stabilization arises from MSCs locked into fibers rather than from the assembled mesophase.

Beyond X-ray scattering and high resolution STEM imaging, the arrangement of MSCs within the fibrous assembly can also be probed by measuring the optical fluorescence anisotropy. Fluorescence (or polarization) anisotropy[44−47] provides a particle-level probe into anisotropy, and the response is likely not influenced by neighboring clusters given the large gap between the MSCs (~2 nm). We observe a strong anisotropic response reaching close to 0.4 near the band gap (Figure 4).

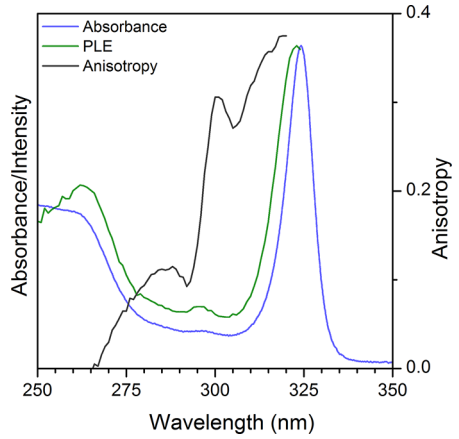

Figure 4. Polarization anisotropy. Comparison of absorbance, photoluminescence excitation (PLE), and photoselection-PLE (PS-PLE or fluorescence anisotropy). In contrast to the isotropic emission typical in spherical NPs, MSCs show linearly polarized emission more similar to elongated nanorods. PLE was measured specifically at 331 ± 1 nm to characterize only transitions related to the main PL peak of the MSCs.

The 0.4 value corresponds to a linearly polarized and parallel absorption and fluorescence transition dipole moment. This result indicates that the allowed electronic transitions of the MSCs are anisotropic, which implies that their crystal structure is anisotropic as well (Figure 4 and S5). Comparing the MSCs anisotropy properties to larger CdS NCs with the same crystal structure shows they are more similar to elongated nanorods (NRs) with linearly polarized emission, rather than to spherical NPs that show isotropic emission in solutions. For NRs, the linear polarization arises due to their anisotropic structure,[46,48] suggesting that the shape of the MSCs is anisotropic as well. We therefore conclude that the MSCs define the basic building blocks of the fibrous hexagonal assemblies, and that the underlying anisotropy in the MSC promote the fibrous assembly.

***In Situ* Mesophase and MSC Formation.** The combination of small- and wide-angle X-ray scattering (SAXS/WAXS) provides an opportunity to monitor the coevolution of the mesophase and the constituent MSCs in real time (Figure 5). We investigated how the formation of the mesophase and inorganic structures is influenced by precursor concentration (100, 500, 1000 mM) over the course of 5 h at 130 °C (Figure 5 and Figures S6–S9). Below, we describe the coevolution of SAXS and WAXS patterns for each concentration.

For the 1000 mM reaction, the broad SAXS peak ($Q \sim 0.27$ Å^{-1}) decays in intensity over time, whereas a new set of SAXS and WAXS peaks emerge and increase in intensity (Figure 5a). The broad decaying SAXS peak ($Q \sim 0.27$ Å^{-1}, 2 nm *d*-spacing) originates from the cadmium oleate precursor (Figure S7), which is likely a micellar phase as previously seen at high concentrations.[49] The spacings of the narrow hexagonal mesophase (SAXS) peaks stay constant while their peak intensity increases with time, indicating an increased abundance of a singular mesophase in solution. The intensity of the mesophase peaks increase concurrently with the intensity of the

DOI: 10.1021/jacs.7b12175
J. Am. Chem. Soc. 2018, 140, 3652−3662

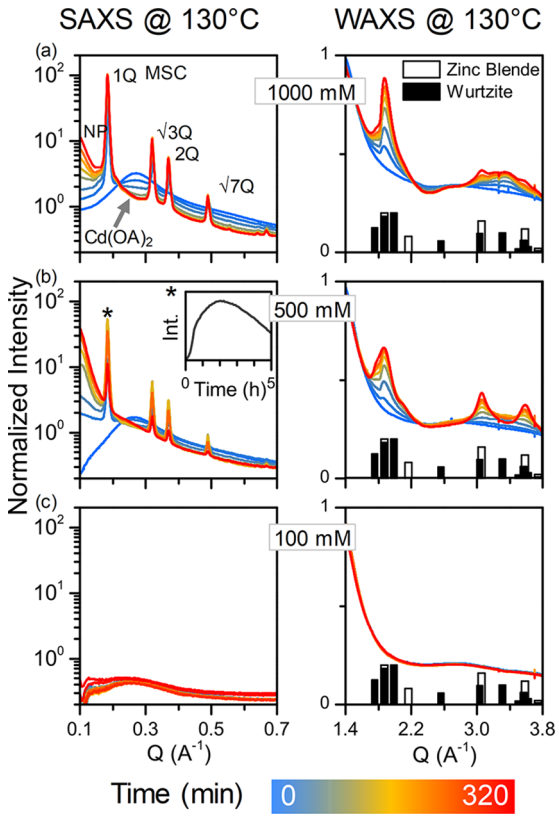

Figure 5. *In situ* mesophase and MSC formation. *In situ* SAXS and WAXS at 130 °C for magic-sized clusters prepared at three different metal precursor concentrations (1000, 500, 100 mM). (a) In the 1000 mM case, the data shows formation of MSCs (WAXS) with assembly into a large hexagonal mesophase (SAXS). (b) 500 mM reaction initially forms a hexagonal assembly (SAXS), which fades at longer times when NP formation increases (WAXS). (Inset) Intensity over time for peak at 1Q, which corresponds to mesophase assembly. (c) For the 100 mM reaction, no CdS reaction is observed.

broad WAXS MSC peaks, suggesting that formation of MSCs is inherently coupled to the mesophase formation. Similar behavior is observed at the maximum or neat cadmium oleate concentration reaction (i.e., 1580 mM at 130 °C) (Figure S10).

By comparison, the scattering signature of the synthesis at 500 mM is similar to the 1000 mM reaction, i.e., narrow SAXS and broad WAXS peaks emerge and increase with time. However, at longer times (>2 h) the narrow mesophase peaks begin to fade, while the low-Q (0.1−0.2 $Å^{-1}$) structure factor changes slope, and sharper WAXS peaks appear (Figure 5b). The increasing slope at low-Q indicates an increase in the particle size (Figure S11). Interestingly, the sharper WAXS peaks align better with the ZB phase of CdS, in contrast to the WZ-like structures observed for the MSCs at high concentrations. Specifically, the ZB peaks at 3.1 and 3.6 $Å^{-1}$ ((220) and (311) diffraction planes; 44.0° and 52.1° 2θ for Cu K-α source, respectively) appear while a WZ peak at 3.3 $Å^{-1}$ ((103) plane; 47.8° 2θ for Cu K-α source) fades.

At conventional concentrations (100 mM), no change in intensity or peak formation is observed in the SAXS or WAXS (Figure 5c). The transformation between the fibrous mesophase and NP growth at 500 mM implies the higher selectivity for MSC at 1000 mM is a result of the MSC fibrous assemblies, which likely impede the onset of the NP growth.

The evolution of the MSC and mesophase structure evident from the SAXS/WAXS results summarized in Figure 5 led us to hypothesize that the stability of the MSCs in the high-concentration environment derives from the clusters being assembled into fibers and encapsulated within a fibrous surfactant mesophase. The arrangement of MSCs within the fibrous mesophase limits the mobility of the nuclei and effectively freezes or isolates them from the surrounding reaction environment. Whereas the conventional mantra has been that the stability of MSCs derives from the precise arrangement of the inorganic structures (i.e., closed-shell atomic packing),[23,24,50] we demonstrate that anisotropic clusters can also be stabilized within fibrous assemblies. We note that the lack of strong order within the MSC building blocks studied here is consistent with a recently isolated stable nanocluster that has a disordered structure, and is hypothesized to be stabilized by interconnected networks of surface ligands.[29,51] Collectively, these results underscore that higher concentrations promote not only the formation of MSCs in high purity, but also generate liquid-crystalline fibrous mesophase assemblies. These assemblies afford an additional level of stabilization for the clusters at high concentrations.

By tracking characteristic peaks in SAXS and WAXS during the synthesis we can directly compare the structural evolution of the inorganic discrete MSCs and their assembly into ordered fibrous ensembles during synthesis (Figure 6). To disentangle the complex interplay between simultaneous atomic, nanoscale, and mesoscale phenomena, we focus on four characteristic peaks corresponding to (I) the first peak for the hexagonal assembly, (II) the cadmium oleate micelles, (III) CdS diffraction peak shared by both ZB and WZ phases (1.87 $Å^{-1}$), and (IV) characteristic ZB and WZ peaks (at 3.07 and 3.37 $Å^{-1}$, respectively) (Figure 6a,b and SI). To highlight the critical effect of the precursor concentration, we compared the 100, 500, and 1000 mM reactions. The 100 mM reaction shows no peak change or MSC formation, hence the normalized intensity is zero and no further analysis was performed. The cadmium oleate micelle peak (II) is initially more pronounced in the 1000 mM reaction, and decays exponentially in both the 500 and 1000 mM reaction (Figure 6c). This indicates that more cadmium oleate micelles form in the 1000 mM as compared to the 500 mM reaction, which is not surprising given the higher concentrations. Notably the cadmium oleate peak for 1000 and 500 mM plateaus at roughly the same time. Concurrently, the hexagonal MSC mesophase peak (I) increases (Figure 6e) along with the slope of the NP structure factor peak at low-Q (Figure S11). In the 1000 mM reaction the hexagonal MSC peak (Figure 6e, red plot) rises and ultimately plateaus in time; but, surprisingly, for the 500 mM reaction this peak reaches a maximum, and then decays with time (Figure 6e, purple data set). The mesophase structure is roughly twice as abundant in the 1000 mM reaction compared to 500 mM at 2 h.

These real-time *in situ* studies reveal that the formation of the MSC SAXS assembly peak coincides with the formation of several broad peaks in the WAXS, which are characteristic CdS diffraction planes. The loss of MSC assemblies in the 500 mM reaction and not in the 1000 mM, highlights the stability supplied by the hexagonal surfactant mesophase. This stability degrades upon prolonged exposure to higher free acid concentrations (in the 500 mM reaction), akin to an Ostwald ripening mechanism for NP, or exposure to higher temperatures, which promote NP growth (see Figure S12 1000 mM

DOI: 10.1021/jacs.7b12175
J. Am. Chem. Soc. 2018, 140, 3652−3662

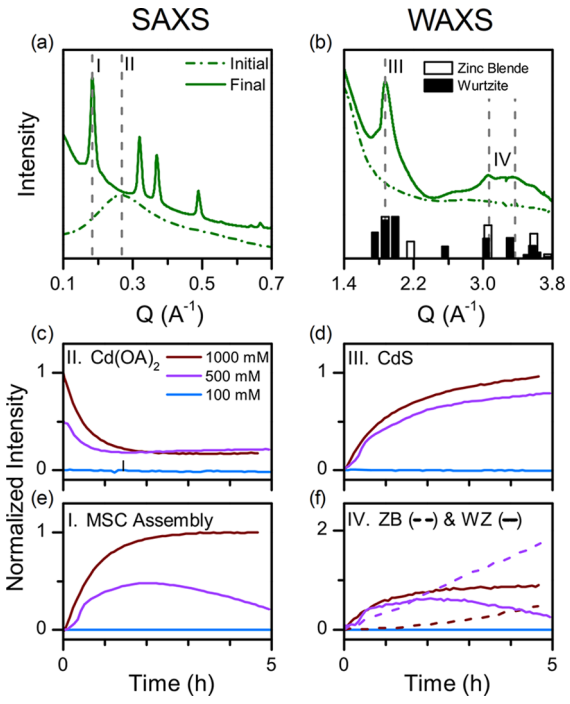

Figure 6. Time-resolved X-ray analysis. Comparison of initial and final patterns for 1000 mM synthesis at 130 °C, (a) SAXS and (b) WAXS with enumerated characteristic peaks (I–IV). (c–f) Comparison of the evolution of reactant and product peaks at 130 °C for three different precursor concentrations: 100, 500, 1000 mM (see SI for details on analysis). (c) The Cd-oleate micelle peak (II) decreases, and then plateaus over the course of the reaction. (d) CdS diffraction peak (a shared ZB and WZ peak, 1.87 $Å^{-1}$, labeled (III)), increases with time indicating that the loss of Cd-oleate corresponds to the formation of CdS. (e) The intensity of the sharp 1Q hexagonal MSC assembly peak (I) increases with time for the 500 and 1000 mM reactions, but not for the 100 mM reaction. This peak begins to fade away at longer times in the 500 mM, but not the 1000 mM reaction. (f) Intensity of characteristic ZB (- -) and WZ (—) peaks at 3.07 and 3.37 $Å^{-1}$, respectively (labeled (IV)). For the 1000 mM, the formation of the MSCs mirrors the WZ peak intensity. For 500 mM, the loss of WZ MSC intensity with time mirrors the decay of the MSC assembly, and is accompanied by linearly increasing ZB intensity from NPs growing at the expense of MSCs. Though the ZB peak overlaps with a WZ peak, the fact that this peak increases, while a unique WZ peak decreases, suggests the increase in peak intensity is due to ZB formation.

reaction at 175 °C). Though previous results suggest the closed-shell stability of MSC prevents Ostwald ripening (partial dissolution),[30,52] the loss of MSCs at 500 mM implies that individual MSCs completely dissolve into monomers and surfactants to grow NPs. While both conditions (500 and 1000 mM) form CdS MSCs with mesophase assemblies, the 1000 mM concentration is significantly more resistant to mesophase degradation and NP growth.

Closer inspection of the WAXS measurements provides important insight into the transition from MSC nucleation to NP growth. We compared the formation and phase of the CdS by tracking a shared ZB/WZ peak and characteristic ZB-only and WZ-only peaks. Figure 6d shows that over the same reaction time, broad CdS diffraction peaks (III) increase for both the 500 mM and 1000 mM reactions, but more significantly for the 1000 mM reaction. The growth of the WAXS signature (Figure 6d), indicating the formation of small CdS crystallites, and the concomitant decay of the Cd oleate micelle signature (Figure 6c) suggest that the two processes are related. As previously discussed, the MSCs are more WZ-like whereas the NPs are more ZB-like. At longer times (>1 h), the intensity of the ZB peak increases due to NPs growth (Figure 6f, dashed lines). The ZB peak intensity increases more rapidly in the 500 mM compared to the 1000 mM reaction (Figure 6f, dashed curves). Over the same time (>1 h) in the 500 mM reaction, the characteristic WZ peak of the MSCs begins to decay, whereas the peaks plateau in the 1000 mM reaction (Figure 6f, solid curves). Hence, ZB-like NPs form not only at the expense of the MSC assemblies (Figure 6e) but also at the expense of the MSC WZ-like inorganic phase (Figure 6f). These results highlight that hexagonal MSC assemblies provide a barrier to NP growth that is more pronounced at higher concentration.

DISCUSSION

Access to high-purity MSCs enables us to directly address two fundamental questions with regards to control of MSCs: (1) What is the source of MSC stability against growth? and (2) What are the factors governing the formation of either MSCs or NPs?

MSC Stability and Mesophase Formation. The time-resolved SAXS/WAXS data provide new insights into the origin of MSCs stability. Conventionally, MSCs have been suspected to be stabilized by a symmetric, close-shelled structure that resists atom-by-atom addition (i.e., no low coordination atoms).[23,24,50] However, several groups have demonstrated that different MSCs correspond to differences in surface chemistry rather than size.[33,53] Moreover, other studies have shown that same-sized MSCs can be structural polymorphs[54] or possess atomically disordered structures.[51] Though the small size and intermediate nature of a MSC make it difficult to resolve the underlying structure, these results suggest that the structure of the inorganic core alone may not be the origin of MSCs stability.

In this work, we demonstrate that there is a strong link between a fibrous assembly and MSC stability, by showing that mesophase assembly accompanies MSC formation. Subsequent resuspension and heating of cleaned MSCs highlights that the individual fibers rather than their macroscopic mesophase assembly are the source of MSC stability (see later discussion). The link between MSC self-assembly and stability is reinforced by the observation that degradation of the fibrous mesophase assembly destabilizes the MSCs, and results in the loss of MSCs and the enhancement of NP growth (Figure 6). At high concentration, the fibrous MSCs assembly is retained, and shields (i.e., kinetically arresting) the MSCs against growth. Furthermore, the MSCs are also locked in at a single size, and stabilized against the quantized growth that is often observed between different MSC families (Figure 7).[22,27,30,55] We hypothesize that the MSC fibrous assemblies may be the source of MSCs stability in addition to a symmetric inorganic structure as has been previously proposed.

To investigate the mechanism of growth from (or destabilization of) MSCs into NPs without precursors, (i.e., through Ostwald ripening and/or coalescence),[27] we heated the MSCs in two forms: (1) cleaned and resuspended in 1-octadecene (ODE), and (2) a cleaned solid product (no resuspension in solvent). We monitored the system with SAXS/WAXS. At 100 °C, the concentrated solution of MSCs in ODE (100 mg/mL) did not show a hexagonal mesophase,

DOI: 10.1021/jacs.7b12175
J. Am. Chem. Soc. 2018, 140, 3652–3662

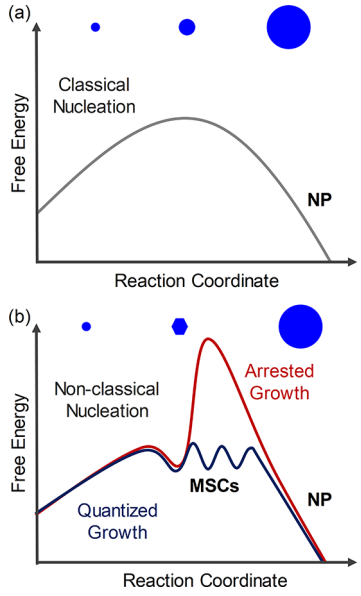

Figure 7. MSC vs NP reaction coordinate. Qualitative comparison of (a) classical and (b) nonclassical nucleation barriers along with growth barriers for quantized MSC growth and the kinetically arrested growth. The formation of a mesophase generates an additional energy barrier, restricting the transition from MSCs formation to NP growth, and locking the MSCs in the nucleation phase.

suggesting that the mesophase completely unbundles upon solvent intercalation to form a fibrous suspension (Figure S13). The persistence of a fibrous suspension is suggested by highly viscous and gel-like solution behavior, and reinforced by the presence of large structural features observed using dynamic light scattering (Figure S14). Heating the resuspended MSC solution to 200 °C did not induce NP growth, highlighting the remarkable stability of the MSCs against growth either by coalescence or ripening. (Figure S13). The resistance of cleaned and resuspended MSCs to growth and dissolution is consistent with a previously published study.[30] MSC stability, in the absence of a mesophase, indicates that the individual fibers of MSCs, and not their mesophase assemblies, are the fundamental source of MSC stability.

For the cleaned solid MSC product experiment (i.e., without solvent), the hexagonal mesophase is observed and retained upon heating to 200 °C, though the mesophase assembly expands by 3% (see Figure S15). Both results of these heating experiments highlight the thermal stability of the fibrous MSCs. The solid-like (high viscosity) nature of hexagonal mesophase, along with the gel-like nature of MSCs in ODE, deters MSC dissolution and growth. On the basis of these monomer-free experiments, we conclude that at typical synthesis temperatures (i.e., 100−200 °C), MSC to NP conversion is not through cluster assembly or a coalescence mechanism when a mesophase or fibrous assembly is present.

Surfactant Phase Behavior in Prior MSC Literature. Several other studies indirectly allude to a connection between surfactant structure and MSC formation. Mesophases have been identified by turbid solutions,[15] and well-defined peaks in the small-angle X-ray scattering,[16,17] and/or optical birefringence.[18] In line with these metrics, several works mention the following in connection with MSC formation: solution turbidity and MSCs self-assembly,[19] and X-ray or NMR detection of large (∼1 nm) micellar aggregates.[20,21] Nevertheless, these works do not connect solution or mesophase structure to the stability of the MSCs.

There may be a more fundamental connection between MSCs and mesophases through supersaturation. Previous studies indicate that high levels of monomer supersaturation promote MSC formation.[22,26] Based on the micelle theory, high levels of surfactant supersaturation (relative to critical micelle temperature/concentration) promote micelle or mesophase formation. Thus, sufficiently low temperatures or high concentrations may promote both the formation of MSCs and mesophases. Previously, the high supersaturation needed for MSC formation is achieved by lower synthesis temperatures (in some cases, <100 °C),[11,12,14,21,22,28,29] and low acid-to-metal ratio (∼3).[19,25,30−32] For example, at a low synthesis temperature (<100 °C), Buhro and co-workers explicitly mention that CdSe MSCs form within a lamellar surfactant mesophase composed of the precursors.[11,12,14] Another recent low-temperature study demonstrated that perovskite nanoclusters ($CsPbBr_3$) are characterized by a milky solution, and stabilized by mesophase formation.[56] Together with our results, these findings generalize the importance of mesophase formation and stabilization across a diverse set of cluster syntheses.

At low temperature or low acid concentrations, interactions between metal surfactants are intensified, and may promote the formation of mesophase assemblies. Additionally, as suggested by micelle theory, high concentration can also promote mesophase formation. A recent paper showed that using high concentration, "solvent-free" conditions directs the reaction pathway from NP to nanoplatelet formation, and no mesophase was observed.[57] Three other studies synthesized metal carboxylates, under what we classify as high concentrations (500, 570, and 830 mM), but then diluted the precursors to conventional concentrations prior to MSC synthesis (to 120, ∼120, and 250 mM, respectively), and did not mention the high concentration preparation as necessary for MSC formation, even though surfactant behavior is concentration-dependent with high concentrations promoting micelle and mesophase formation.[21,30,31] Taken together, these results imply that many previous MSC studies may have been, unknowingly, observing mesophase or surfactant structure formation coupled with MSC formation.

MSC vs NP Formation. The ratio of organic surfactant to metal plays a critical role in switching the synthetic pathway between MSCs and NPs. Based on our results (Figure 6 and S16) and previous literature reports, the estimated crossover point from NP to MSC formation is an acid/Cd ratio of <16, which corresponds to a free acid vs total acid or oleate percentage of <87%.[32,58] Specifically, we find that for acid-to-metal ratios ≤16 (i.e., metal concentration ≥ 200 mM), MSCs form in larger number than NPs. Previous reports mention that low acid-to-metal ratios (∼3), even at low precursor concentrations (20 mM, diluted with ODE),[19,30−32,58] promote MSC formation, and MSCs are detected up to an acid-to-metal ratio of 10.[32,58] At lower acid/Cd ratios, there is less free surfactant to stabilize/disperse the metal precursor; thus, precursor-precursor (i.e., cadmium oleate) self-interactions are preferred over solvent/surfactant interactions, promoting the formation of precursor solution structure (e.g., micelles). We propose that these precursor-precursor interactions provide a stronger driving force for MSC formation over NPs, and are more prevalent at high concentrations. Though low acid/Cd ratios, even at dilute conditions, are sufficient to promote MSC

DOI: 10.1021/jacs.7b12175
J. Am. Chem. Soc. 2018, 140, 3652−3662

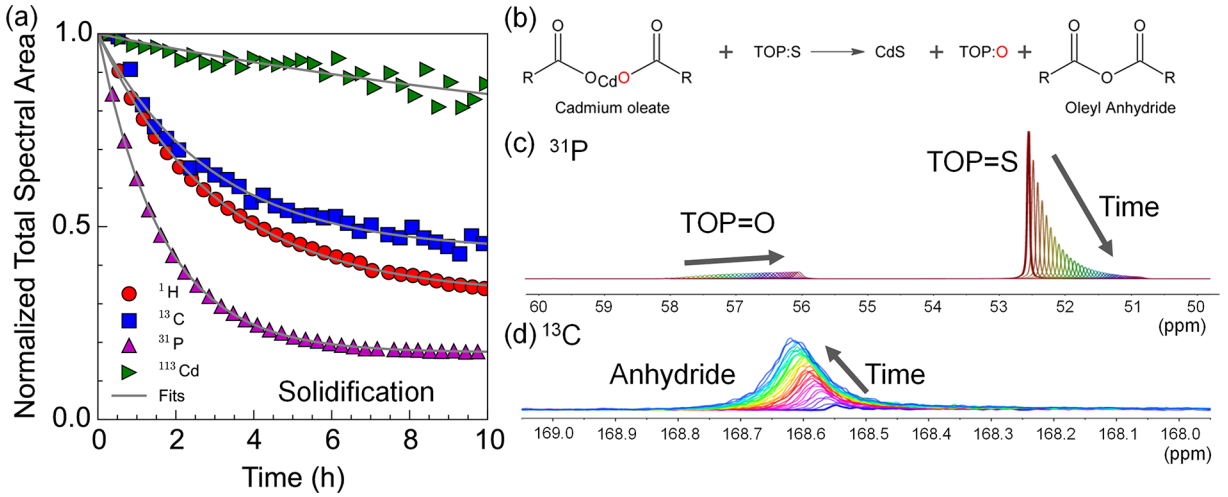

Figure 8. 1000 mM Synthesis at 130 °C (NMR). (a) The total spectral area of the four nuclei investigated decreases with time (H, C, P, and Cd). The silencing of the signal is attributed to species becoming NMR inactive through solidification.[75−77] (see Table S5). (b) Reaction schematic showing the conversion from precursor (Cd-oleate and TOP=S) to CdS along with organic byproducts (TOP=O and oleyl anhydride). (c) ^{31}P NMR spectrum showing the emerging peak (between 58 and 56 ppm), which is assigned to TOP=O formation while the initially more intense, but decreasing, peak (between (52.5 and 50.5 ppm) is assigned to TOP=S (from literature 48.5 to 50.2 ppm values are observed for TOP=O and 48.6 pm for TOP=S, respectively).[73] It is known that P peaks can shift in the presence of Lewis acid (which could include oleic acid and possible cadmium oleate). (d) ^{13}C NMR spectrum showing the emergence of an oleyl anhydride peak ($(-CH_2CO)_2O$) that increases with time, and is at a similar location (168 ppm) to previously reported oleyl anhydride peak.[73]

formation, only high concentrations suppress NP growth (Figure S17).

We observe that MSCs transition into NP at longer times, high temperatures, or upon addition of coordinating solvents to the 1000 mM reaction. Several other common synthesis parameters (stoichiometry, ramp rate, and ligand length) did not affect the 324 nm MSC formation, hexagonal mesophase formation, or MSC into NP growth (see Figures S18−S23). As was previously shown (Figure 5), both 500 and 1000 mM cadmium oleate concentrations generate MSCs and a hexagonal mesophase. At longer reaction times for the 500 mM reaction, the mesophase and MSCs decay while NPs grow (see Figure 5 and Figure S1), resembling the Ostwald ripening mechanism which is known to occur at high free acid concentrations.[4] Increasing the reaction temperature also leads to the formation of NPs, and the loss of the hexagonal mesophase and MSCs, but no transformation to a different mesophase structure (Figure S13). These results indicate that MSCs destabilize, and degrade, as they transition to NPs, and that MSC to NP conversion is predominately through monomer-driven growth, not cluster coalescence.

Precursor or MSC Templated Mesophase Formation. The driving force behind the mesophase formation is the assembly of MSCs and/or precursor templating. The anisotropic shape of MSCs (Figure 4) and the fact that identical fibrous MSCs form, regardless of precursor chain length (Figure S22), suggests that the inorganic core is driving the fibrous assembly. Nevertheless, there is some contribution from the cadmium oleate. To better understand the role of free solvent on cadmium oleate structure, we cleaned 1000 mM cadmium oleate from the free oleic acid, and resuspended the neat cadmium oleate at 1000 mM concentration in several different solvents: ODE, oleylamine, trioctylphosphine oxide (TOP=O), and dodecanol. Then, TOP=S was injected and the solution was heated to 130 °C. Reaction in a noncoordinating solvent (ODE) yields similar results to the original 1000 mM synthesis reaction: only MSCs are formed along with a hexagonal assembly (Figure S24−S26). For coordinating solvents, only the dodecanol formed MSCs with a hexagonal assembly, and also some NP growth, whereas oleylamine and TOP=O produce mainly large NPs without any significant mesophase (Figure S24−S26). The addition of coordinating solvents disrupts the cadmium oleate coordination,[59] and reveals that the solution structure of not only the MSCs but also the cadmium oleate precursor is essential to stabilize the MSCs, and the mesophase, and deter NP growth. Recent studies have shown that coordinating solvents also disrupt the ligand networks of individual MSCs,[33,60] indicating that the surfactant/ligand structure is intimately connected with both the formation, stability, and assembly of MSCs.

Metal carboxylates such as the cadmium oleate precursor are well-known within other fields to exhibit solution structure and are classified as heavy metal soaps/surfactants,[6,9,61,62] metallomesogens,[17,49,63−65] metallogels,[66−69] and/or coordination polymers.[59,66,69] Cadmium carboxylates typically form solution structures that can be described as columnar or worm-like micelles, coordination polymers, fibrous metallogel and/or hexagonal mesophases.[10,59,61,69,70] We observe evidence of micelle structure cadmium oleate at 130 °C with a 2.6 nm *d*-spacing ($Q \approx 0.25$ Å^{-1}) (Figure S7). In contrast to the small micellar size of the cadmium oleate (Sherrer size ∼ 10 nm; Figure S7), the MSC mesophase emerges as an extremely narrow peak (100s nm grain) rather than narrowing as the reaction proceeds. This behavior reinforces the idea that cadmium oleate exists as long, worm-like micelles or as a coordination polymer prior to MSC formation. The addition of coordinating solvents alters the micelle structure, and directs the synthesis away from MSCs, and toward NP formation (Figure S26). A recent *in situ* SAXS study (dilute 30 mM cadmium myristate + chalcogenide source at 100 °C) did not show a peak around $Q = 0.25$ Å^{-1}, and reports <1 nm sized micelle.[71] Therefore, only higher concentrations of cadmium oleate increase the interaction probability between individual cadmium oleate surfactant creating larger micelles (or

DOI: 10.1021/jacs.7b12175
J. Am. Chem. Soc. 2018, 140, 3652−3662

coordination polymers) that template MSC formation and assembly. If these precursor structures are disrupted (with coordinating solvents), the MSCs are destabilized, and NP growth ensues. On the basis of these results, we conclude that both the anisotropic shape and precursor structure template the mesophase formation.

Kinetics. Beyond insights into the MSC stability and MSC vs. NP selectivity, the time-resolved SAXS/WAXS experiments also provide new understanding into the kinetics of MSC and NP formation. It is generally postulated that colloidal syntheses require burst nucleation to produce monodisperse particles, and nuclei are treated as unstable and fleeting transition states, quickly overtaken by NP growth.[2,3,72] In contrast, nonclassical syntheses may involve continuous nucleation, and stable and persistent intermediates, or clusters, can be observed.[5,27,29] The ability to isolate and track these crucial reaction intermediates, which often can be MSCs, provides a probe into the nonclassical NP synthetic pathway (and nucleation processes) in a way not achievable in conventional NP syntheses. Specifically, the selectivity for MSCs over NPs, at high concentrations, decouples precursor conversion kinetics that contribute to MSC formation from NP growth.

We probed the precursor kinetics for MSCs using *in situ* NMR and X-ray scattering and *ex situ* absorbance analyses. By following the organic precursor constituents via NMR, we observe a similar precursor conversion mechanism as reported previously by Owen and co-workers,[73,74] in which metal carboxylates react with trioctylphosphine chalcogenides to form TOP=O, oleyl anhydride, and metal chalcogenide monomer (Figure 8 and S27−S29). The resulting metal chalcogenide monomer then nucleates and grows to form MSCs and/or NPs. However, a notable difference in our high concentration synthesis is that some species become NMR silent (i.e., the total spectral area decreases) over the course of the reaction, based on ^{13}C, ^{31}P, and ^{1}H NMR (Figure 8a). This NMR silencing indicates solidification,[75−77] and this process occurs at a similar rate as the formation of the MSCs mesophase ($\sim 10^{-4}$ s^{-1}, see Table S5 and Figure S30). Though the precursor conversion products (i.e., TOP=O and oleyl anhydride) match those in conventional syntheses, synthesis at high concentration involves another process (i.e., phase change, observed as NMR "silencing") that promotes highly selectivity MSCs formation and assembly.

Regarding the inorganic constituents (MSCs and NPs), the *ex situ* absorbance spectra show a linear or zero-order reaction for the MSC formation ($2 \pm 0.1 \times 10^{-6}$ M s^{-1}; see Figure S30). This rate is slower, but similar to precursor conversion during the initial nucleation phase of CdSe NPs at higher temperatures (10^{-5} M s^{-1}),[4] and much slower than the first-order precursor conversion rate that includes NP growth (10^{-3}−10^{-1} s^{-1}).[1,72,73] The linear (or zero-order) relationship between precursor conversion rate and NP production is expected based on classical nucleation theory during the nucleation phase,[1,6,78] indicating that the MSCs are similar to nuclei.[27,29] Nevertheless, our MSCs are locked at a single size and do not grow in contrast to NP nuclei that continuously grow. We observe continuous nucleation of MSCs over an extremely long time (~6 h) compared to typical burst nucleation times (seconds) in conventional synthesis. The prevalent classical understanding is that the burst (short-lived nucleation) is crucial to obtain monodisperse NPs.[3,78] In stark contrast, we show that high concentration synthesis promotes continuous nucleation of clusters and deters NP growth via fibrous assembly and mesophase formation, ultimately supplying a batch of monodisperse clusters.

At longer reaction times, the reaction transitions from MSC nucleation to NP growth for 500 and 1000 mM. The rate of NP formation from *ex situ* absorbance is first order for the 500 mM reaction (6×10^{-4} s^{-1}), whereas no NP formation rate is observed for the 1000 mM reaction (Figure S30). These rates are slower than those previously reported (0.001−0.1 s^{-1}),[1,72,73] though literature values include both nucleation and growth contributions to precursor conversion, and are in less viscous synthesis environments. Generally, the slower rates at high concentrations align with the current understanding of the precursor to monomer conversion leading up to nucleation as the rate limiting reaction step (nucleation rates are slower than growth rates[1,2]) and the lower solution diffusivity at high concentration limits the growth rate.[79−81] The formation of mesophase structure effectively minimizes the solution diffusivity, and thus NP growth, through the formation of a solid (low diffusivity) phase. In effect, the fibrous and mesophase structures at high concentration kinetically arrest or freeze the MSCs, further stabilizing their kinetically persistent structure.

CONCLUSIONS

In summary, we demonstrate that colloidal NP synthesis in the high concentration regime accentuates surfactant phase behavior leading to the formation of high-purity MSCs stabilized within a highly ordered hexagonal mesophases assembly. Our results indicate that the fibrous MSC assemblies are likely templated from structure inherent to the cadmium oleate precursor as well as inherent shape anisotropy of the MSCs. We present a mechanism in which MSCs in the assembly are shielded from further growth (i.e., kinetically arrests NP growth), and propose that MSC assemblies may be the source of MSCs stability rather than, or in addition to, a precise inorganic structure. NP growth can be initiated at the expense of both the MSC and their hexagonal mesophase. NP growth at expense of MSC implies that synthetically MSCs are intermediates or "monomer reservoirs" for NPs rather than NP nuclei. Whereas syntheses at conventional concentrations are governed by monomer-addition-based growth, or monomeric surfactant/precursor environments, we establish that high precursor concentrations expand the colloidal phase diagram for NP synthesis into more complex surfactant phase behavior, namely micelles and mesophases. Though inorganic phase change (e.g., nucleation) is fundamental to NP synthesis, the importance of innate organic phase change (e.g., surfactant mesophase formation) has been latent and underappreciated. This organic phase behavior is revealed in the new high concentration regime that is characterized by maximizing precursor−precursor interactions to form a solution structure that selectively navigates the synthetic pathway to isolate high-purity MSCs. In contrast, conventional concentrations are more sensitive to other chemical interactions with the precursors (including solvent, surrounding defects, impurities). High concentration NP syntheses selectively control the predominant molecular interactions during NP syntheses. Insight into inherent surfactant phase behavior of NP precursors as metal soaps provides a generalized framework for metal chalcogenide and perovskite NP synthesis. Overall, the high-concentration synthesis regime accentuates fundamental surfactant phase behavior, and offers a generalized method for synthesizing,

DOI: 10.1021/jacs.7b12175
J. Am. Chem. Soc. 2018, 140, 3652−3662

stabilizing, and studying high-purity metal chalcogen clusters that are persistent intermediates in nonclassical NPs syntheses.

■ ASSOCIATED CONTENT

Supporting Information

The Supporting Information is available free of charge on the ACS Publications website at DOI: 10.1021/jacs.7b12175.

Synthesis procedure and characterization methods; X-ray analysis methods (including peak tracking, structure factor, Scherrer analysis); absorbance and SAXS/WAXS for 500 and 1000 mM time series; additional STEM images; 1000 mM synthesis at higher temperature and with different free solvents (SAXS/WAXS); SAXS/WAXS while heating resuspended MSCs and solid MSCs; high concentration synthesis with different carboxylic acid ligands (SAXS/WAXS); kinetic fits to absorption, X-ray and NMR data (PDF)

■ AUTHOR INFORMATION

Corresponding Authors

*th358@cornell.edu
*rdr82@cornell.edu

ORCID

Douglas R. Nevers: 0000-0003-2574-1852
Ido Hadar: 0000-0003-0576-9321
Uri Banin: 0000-0003-1698-2128
Tobias Hanrath: 0000-0001-5782-4666
Richard D. Robinson: 0000-0002-0385-2925

Author Contributions

§These authors contributed equally.

Notes

The authors declare no competing financial interest.

■ ACKNOWLEDGMENTS

This work was supported in part by the National Science Foundation (NSF) under Award No. CMMI-1344562. U.B. acknowledges funding for this project from the European Research Council (ERC) under the European Union's Horizon 2020 research and innovation programme (grant agreement no. 741767). U.B. also thanks the Alfred & Erica Larisch memorial chair. B.H.S. and L.F.K. acknowledge support by the Packard Foundation. B.H.S was supported by NSF GRFP grant DGE-1144153. This work also made use of the Cornell Center for Materials Research Shared Facilities, which are supported through the NSF MRSEC (Materials Research Science and Engineering Centers) program (Grant DMR-1719875). The FEI Titan Themis 300 was acquired through NSF-MRI-1429155, with additional support from Cornell University, the Weill Institute and the Kavli Institute at Cornell. This work includes research conducted at the Cornell High Energy Synchrotron Source (CHESS), which is supported by the National Science Foundation and the National Institutes of Health/National Institute of General Medical Sciences under NSF award DMR-1332208. Dynamic light scattering measurements were performed in a facility supported by Award No. KUS-C1-018-02, made by King Abdullah University of Science and Technology (KAUST). This work made use of the Cornell Chemistry NMR Facility, which is supported in part by the NSF-MRI grant CHE-1531632. R.D.R. thanks the U.S. Fulbright Scholar Program for partial funding during this work. The authors thank the following individuals for assistance with experiments and material characterization as well as useful discussion. Specifically, Detlef Smilgies provided equipment and helpful discussion regarding the X-ray scattering experiments. Stan Stoupin set up and calibrated the beamline and detector for SAXS/WAXS, and helped with data analysis. Ivan Keresztes performed the NMR data acquisition, helped with analysis, and provided useful guidance.

■ REFERENCES

(1) Hendricks, M. P.; Campos, M. P.; Cleveland, G. T.; Plante, I. J.; Owen, J. S. *Science* **2015**, *348*, 1226−1230.
(2) Hens, Z.; Čapek, R. K. *Coord. Chem. Rev.* **2014**, *263*−*264*, 217−228.
(3) Kwon, S. G.; Hyeon, T. *Small* **2011**, *7*, 2685−2702.
(4) Owen, J. S.; Chan, E. M.; Liu, H.; Alivisatos, A. P. *J. Am. Chem. Soc.* **2010**, *132*, 18206−18213.
(5) Lee, J.; Yang, J.; Kwon, S. G.; Hyeon, T. *Nat. Rev. Mater.* **2016**, *1*, 16034.
(6) García-Rodríguez, R.; Hendricks, M. P.; Cossairt, B. M.; Liu, H.; Owen, J. S. *Chem. Mater.* **2013**, *25*, 1233−1249.
(7) Anderson, N. C.; Hendricks, M. P.; Choi, J. J.; Owen, J. S. *J. Am. Chem. Soc.* **2013**, *135*, 18536−18548.
(8) Boles, M. A.; Ling, D.; Hyeon, T.; Talapin, D. V. *Nat. Mater.* **2016**, *15*, 141−154.
(9) Pilpel, N. *Chem. Rev.* **1963**, *63*, 221−234.
(10) Akanni, M. S.; Okoh, E. K.; Burrows, H. D.; Ellis, H. A. *Thermochim. Acta* **1992**, *208*, 1−41.
(11) Liu, Y. H.; Wang, F.; Wang, Y.; Gibbons, P. C.; Buhro, W. E. *J. Am. Chem. Soc.* **2011**, *133*, 17005−17013.
(12) Wang, Y.; Liu, Y.-H.; Zhang, Y.; Wang, F.; Kowalski, P. J.; Rohrs, H. W.; Loomis, R. A.; Gross, M. L.; Buhro, W. E. *Angew. Chem., Int. Ed.* **2012**, *51*, 6154−6157.
(13) Bryks, W.; Smith, S. C.; Tao, A. R. *Chem. Mater.* **2017**, *29*, 3653−3662.
(14) Wang, Y.; Zhang, Y.; Wang, F.; Giblin, D. E.; Hoy, J.; Rohrs, H. W.; Loomis, R. A.; Buhro, W. E. *Chem. Mater.* **2014**, *26*, 2233−2243.
(15) Porter, R. S.; Barrall, E. M.; Johnson, J. F. *Acc. Chem. Res.* **1969**, *2*, 53−58.
(16) Vold, R. D.; Hattiangdi, G. S. *Ind. Eng. Chem.* **1949**, *41*, 2311−2320.
(17) Nelson, P. N.; Taylor, R. A. *Appl. Petrochem. Res.* **2014**, *4*, 253−285.
(18) Khoo, I.-C. *Liquid Crystals: Physical Properties and Nonlinear Optical Phenomena*, 2nd ed.; John Wiley & Sons: New York, 2007.
(19) Yu, K.; Ouyang, J.; Zaman, M. B.; Johnston, D.; Yan, F. J.; Li, G.; Ratcliffe, C. I.; Leek, D. M.; Wu, X.; Stupak, J.; Jakubek, Z.; Whitfield, D. *J. Phys. Chem. C* **2009**, *113*, 3390−3401.
(20) Liu, M.; Wang, K.; Wang, L.; Han, S.; Fan, H.; Rowell, N.; Ripmeester, J. A.; Renoud, R.; Bian, F.; Zeng, J.; Yu, K. *Nat. Commun.* **2017**, *8*, 15467.
(21) Zhu, T.; Zhang, B.; Zhang, J.; Lu, J.; Fan, H.; Rowell, N.; Ripmeester, J. A.; Han, S.; Yu, K. *Chem. Mater.* **2017**, *29*, 5727−5735.
(22) Harrell, S. M.; McBride, J. R.; Rosenthal, S. J. *Chem. Mater.* **2013**, *25*, 1199−1210.
(23) Xie, R.; Li, Z.; Peng, X. *J. Am. Chem. Soc.* **2009**, *131*, 15457−15466.
(24) Jiang, Z. J.; Kelley, D. F. *ACS Nano* **2010**, *4*, 1561−1572.
(25) Evans, C. M.; Love, A. M.; Weiss, E. A. *J. Am. Chem. Soc.* **2012**, *134*, 17298−17305.
(26) Yu, K. *Adv. Mater.* **2012**, *24*, 1123−1132.
(27) Friedfeld, M. R.; Stein, J. L.; Cossairt, B. M. *Inorg. Chem.* **2017**, *56*, 8689−8697.
(28) Beecher, A. N.; Yang, X.; Palmer, J. H.; Lagrassa, A. L.; Juhas, P.; Billinge, S. J. L.; Owen, J. S. *J. Am. Chem. Soc.* **2014**, *136*, 10645−10653.
(29) Cossairt, B. M. *Chem. Mater.* **2016**, *28*, 7181−7189.

DOI: 10.1021/jacs.7b12175
J. Am. Chem. Soc. 2018, 140, 3652−3662

(30) Kudera, S.; Zanella, M.; Giannini, C.; Rizzo, A.; Li, Y.; Gigli, G.; Cingolani, R.; Ciccarella, G.; Spahl, W.; Parak, W. J.; Manna, L. *Adv. Mater.* **2007**, *19*, 548−552.
(31) Yu, Q.; Liu, C.-Y. *J. Phys. Chem. C* **2009**, *113*, 12766−12771.
(32) Yu, W. W.; Peng, X. *Angew. Chem., Int. Ed.* **2002**, *41*, 2368−2371.
(33) Nevers, D. R.; Williamson, C. B.; Hanrath, T.; Robinson, R. D. *Chem. Commun.* **2017**, *53*, 2866−2869.
(34) Yu, W. W.; Qu, L.; Guo, W.; Peng, X. *Chem. Mater.* **2003**, *15*, 2854−2860.
(35) Vossmeyer, T.; Reck, G.; Schulz, B.; Katsikas, L.; Weller, H. *J. Am. Chem. Soc.* **1995**, *117*, 12881−12882.
(36) Tuerk, T.; Resch, U.; Fox, M. A.; Vogler, A. *J. Phys. Chem.* **1992**, *96*, 3818−3822.
(37) Okano, K.; Hayashi, T. *Jpn. J. Appl. Phys.* **1998**, *37*, L177−L179.
(38) Zheng, N.; Bu, X.; Lu, H.; Zhang, Q.; Feng, P. *J. Am. Chem. Soc.* **2005**, *127*, 11963−11965.
(39) Herron, N.; Suna, A.; Wang, Y. *J. Chem. Soc., Dalton Trans.* **1992**, *0*, 2329−2335.
(40) Herron, N.; Calabrese, J. C.; Farneth, W. E.; Wang, Y. *Science* **1993**, *259*, 1426−1428.
(41) Datta, S.; Kabir, M.; Saha-Dasgupta, T.; Sarma, D. D. *J. Nanosci. Nanotechnol.* **2009**, *9*, 5489−5492.
(42) Datta, S.; Kabir, M.; Saha-Dasgupta, T. *Phys. Rev. B: Condens. Matter Mater. Phys.* **2012**, *86*, 115307.
(43) Yeh, C. Y.; Lu, Z. W.; Froyen, S.; Zunger, A. *Phys. Rev. B: Condens. Matter Mater. Phys.* **1992**, *46*, 10086−10097.
(44) Lakowicz, J. R. *Principles of Fluorescence Spectroscopy*, 2nd ed.; Springer US: Boston, MA, 1999; pp 291−319.
(45) Sitt, A.; Salant, A.; Menagen, G.; Banin, U. *Nano Lett.* **2011**, *11*, 2054−2060.
(46) Hu, J.; Li, L.; Yang, W.; Manna, L.; Wang, L.; Alivisatos, A. P. *Science (Washington, DC, U. S.)* **2001**, *292*, 2060−2063.
(47) Tice, D. B.; Weinberg, D. J.; Mathew, N.; Chang, R. P. H.; Weiss, E. A. *J. Phys. Chem. C* **2013**, *117*, 13289−13296.
(48) Hu, J.; Wang, L. W.; Li, L. S.; Yang, W.; Alivisatos, A. P. *J. Phys. Chem. B* **2002**, *106*, 2447−2452.
(49) Liu, C. K.; Warr, G. G. *Soft Matter* **2014**, *10*, 83−87.
(50) Groeneveld, E.; van Berkum, S.; Meijerink, A.; de Mello Donegá, C. *Small* **2011**, *7*, 1247−1256.
(51) Gary, D. C.; Flowers, S. E.; Kaminsky, W.; Petrone, A.; Li, X.; Cossairt, B. M. *J. Am. Chem. Soc.* **2016**, *138*, 1510−1513.
(52) Yu, K.; Hu, M. Z.; Wang, R.; Le Piolet, M.; Frotey, M.; Zaman, M. B.; Wu, X.; Leek, D. M.; Tao, Y.; Wilkinson, D.; Li, C. *J. Phys. Chem. C* **2010**, *114*, 3329−3339.
(53) Cossairt, B. M.; Owen, J. S. *Chem. Mater.* **2011**, *23*, 3114−3119.
(54) Jensen, K. M. Ø.; Juhas, P.; Tofanelli, M. A.; Heinecke, C. L.; Vaughan, G.; Ackerson, C. J.; Billinge, S. J. L. *Nat. Commun.* **2016**, *7*, 11859.
(55) Zanella, M.; Abbasi, A. Z.; Schaper, A. K.; Parak, W. J. *J. Phys. Chem. C* **2010**, *114*, 6205−6215.
(56) Xu, Y.; Zhang, Q.; Lv, L.; Han, W.; Wu, G.; Yang, D.; Dong, A. *Nanoscale* **2017**, *9*, 17248−17253.
(57) Riedinger, A.; Ott, F. D.; Mule, A.; Mazzotti, S.; Knüsel, P. N.; Kress, S. J. P.; Prins, F.; Erwin, S. C.; Norris, D. J. *Nat. Mater.* **2017**, *16*, 743−748.
(58) Li, M.; Ouyang, J.; Ratcliffe, C. I.; Pietri, L.; Wu, X.; Leek, D. M.; Moudrakovski, I.; Lin, Q.; Yang, B.; Yu, K. *ACS Nano* **2009**, *3*, 3832−3838.
(59) García-Rodríguez, R.; Liu, H. *Chem. Commun.* **2013**, *49*, 7857.
(60) Gary, D. C.; Petrone, A.; Li, X.; Cossairt, B. M. *Chem. Commun.* **2017**, *53*, 161−164.
(61) Peng, J. B.; Foran, G. J.; Barnes, G. T.; Gentle, I. R. *Langmuir* **1997**, *13*, 1602−1606.
(62) Corkery, R. W. *Phys. Chem. Chem. Phys.* **2004**, *6*, 1534−1546.
(63) Klimusheva, G.; Mirnaya, T.; Garbovskiy, Y. *Liq. Cryst. Rev.* **2015**, *3*, 28−57.
(64) Serrano, J. L. In *Metallomesogens: Synthesis, Properties, and Applications*; Serrano, J. L., Ed.; WILEY-VCH Verlag GmbH: New York, 1996; pp 1−21.
(65) Barbera, J. In *Metallomesogens: Synthesis, Properties, and Applications*; Serrano, J. L., Ed.; WILEY-VCH Verlag GmbH: New York, 1996; pp 325−348.
(66) Piepenbrock, M. O.; Lloyd, G. O.; Clarke, N.; Steed, J. W. *Chem. Rev.* **2010**, *110*, 1960−2004.
(67) Zhang, J.; Su, C.-Y. *Coord. Chem. Rev.* **2013**, *257*, 1373−1408.
(68) Zhu, L.; He, J.; Wang, X.; Li, D.; He, H.; Ren, L.; Jiang, B.; Wang, Y.; Teng, C.; Xue, G.; Tao, H. *Nanoscale Res. Lett.* **2017**, *12*, 30.
(69) Shi, C.; Zhu, J. *Chem. Mater.* **2007**, *19*, 2392−2394.
(70) Akanni, M. S.; Abass, N. A. *Liq. Cryst.* **1989**, *6*, 597−608.
(71) Abécassis, B.; Bouet, C.; Garnero, C.; Constantin, D.; Lequeux, N.; Ithurria, S.; Dubertret, B.; Pauw, B. R.; Pontoni, D. *Nano Lett.* **2015**, *15*, 2620−2626.
(72) Abe, S.; Čapek, R. K.; De Geyter, B.; Hens, Z. *ACS Nano* **2012**, *6*, 42−53.
(73) Liu, H.; Owen, J. S.; Alivisatos, A. P. *J. Am. Chem. Soc.* **2007**, *129*, 305−312.
(74) Hendricks, M. P.; Cossairt, B. M.; Owen, J. S. *ACS Nano* **2012**, *6*, 10054−10062.
(75) Mauro, M.; De Paoli, G.; Otter, M.; Donghi, D.; D'Alfonso, G.; De Cola, L. *Dalt. Trans.* **2011**, *40*, 12106−12116.
(76) Sanna, C.; La Mesa, C.; Mannina, L.; Stano, P.; Viel, S.; Segre, A. *Langmuir* **2006**, *22*, 6031−6041.
(77) Iqbal, S.; Rodriguez-LLansola, F.; Escuder, B.; Miravet, J. F.; Verbruggen, I.; Willem, R. *Soft Matter* **2010**, *6*, 1875−1878.
(78) Sugimoto, T.; Shiba, F.; Sekiguchi, T.; Itoh, H. *Colloids Surf., A* **2000**, *164*, 183−203.
(79) Williamson, C. B.; Nevers, D. R.; Hanrath, T.; Robinson, R. D. *J. Am. Chem. Soc.* **2015**, *137*, 15843−15851.
(80) Abe, S.; Capek, R. K.; De Geyter, B.; Hens, Z. *ACS Nano* **2013**, *7*, 943−949.
(81) De Nolf, K.; Capek, R. K.; Abe, S.; Sluydts, M.; Jang, Y.; Martins, J. C.; Cottenier, S.; Lifshitz, E.; Hens, Z. *J. Am. Chem. Soc.* **2015**, *137*, 2495−2505.

DOI: 10.1021/jacs.7b12175
J. Am. Chem. Soc. 2018, 140, 3652−3662